Check for updates

Inhibitory Control and the Structural Parcelation of the Right Inferior Frontal Gyrus

Rune Boen[1,2,3], Liisa Raud[4,5] and Rene J. Huster[1,4,6]*

[1] Multimodal Imaging and Cognitive Control Lab, Department of Psychology, University of Oslo, Oslo, Norway, [2] Department of Medical Genetics, Oslo University Hospital, Oslo, Norway, [3] NORMENT, Division of Mental Health and Addiction, Oslo University Hospital and Institute of Clinical Medicine, University of Oslo, Oslo, Norway, [4] Cognitive and Translational Neuroscience Cluster, Department of Psychology, University of Oslo, Oslo, Norway, [5] Center for Lifespan Changes in Brain and Cognition, Department of Psychology, University of Oslo, Oslo, Norway, [6] Sleep Unit, Department of Otorhinolaryngology/Head and Neck Surgery, Lovisenberg Diakonale Hospital, Oslo, Norway

The right inferior frontal gyrus (rIFG) has most strongly, although not exclusively, been associated with response inhibition, not least based on covariations of behavioral performance measures and local gray matter characteristics. However, the white matter microstructure of the rIFG as well as its connectivity has been less in focus, especially when it comes to the consideration of potential subdivisions within this area. The present study reconstructed the structural connections of the three main subregions of the rIFG (i.e., pars opercularis, pars triangularis, and pars orbitalis) using diffusion tensor imaging, and further assessed their associations with behavioral measures of inhibitory control. The results revealed a marked heterogeneity of the three subregions with respect to the pattern and extent of their connections, with the pars orbitalis showing the most widespread inter-regional connectivity, while the pars opercularis showed the lowest number of interconnected regions. When relating behavioral performance measures of a stop signal task to brain structure, the data indicated an association between the dorsal opercular connectivity and the go reaction time and the stopping accuracy.

Keywords: structural parcelation, right inferior frontal gyrus, inhibitory control, response execution, response inhibition

INTRODUCTION

The right inferior frontal gyrus (rIFG) is considered a key node for the inhibition of premature or no longer appropriate motor responses, which is one of the core aspects of behavioral flexibility and control (Swann et al., 2012; Aron et al., 2014, 2016). The IFG represents a structurally diverse area in the prefrontal cortex that usually is divided into three sub-regions based on its cytoarchitecture: the pars opercularis, pars triangularis, and pars orbitalis. Given that variability in the structural architecture of the brain often relates to specific aspects of behavior (Johansen-Berg, 2010), it is likely that the rIFG exhibits a richer functional diversity than often posited. A recent meta-analysis identified different functional clusters of the rIFG to be involved in distinct large-scale networks; only the posterior part (roughly corresponding to the pars opercularis) seemed to be involved in motor control, and was further divided into dorsal and ventral regions associated with response initiation and general inhibition, respectively (Hartwigsen et al., 2019). However, a structural connectivity map of rIFG subregions that would support this functional parcelation is lacking.

The rIFG has been suggested to be part of a right-lateralized fronto-basal ganglia network (Chambers et al., 2009; Jahanshahi et al., 2015), that instantiates inhibition of the motor cortex jointly with the pre-supplementary motor area (preSMA), the basal ganglia, and thalamic nuclei (Aron et al., 2014). Structural and functional connections have been established between the IFG, the preSMA (Swann et al., 2012), subthalamic nucleus (STN), and striatum (Isaacs et al., 2018). While the specific roles of the rIFG and the preSMA for response inhibition are not fully understood, increased fractional anisotropy (FA) in the pars opercularis has been negatively associated with inhibitory performance in a stopping task (i.e., shorter stop signal reaction times), while the reverse association has been reported for the preSMA (Xu et al., 2016). However, the relationship between rIFG and preSMA during inhibitory control is still unclear. It is therefore of fundamental importance to map the structural architecture of those regions that facilitate stopping of behavior in order to fully understand the functionality of the stopping network.

The stop signal task (SST) is one of the most widely used paradigms to study response inhibition, and is often considered the most direct measure of reactive inhibition (van Belle et al., 2014), due to the possibility of calculating the stop signal reaction time (Logan et al., 1984). Yet, the SST additionally provides behavioral measures related to motor preparation under cognitive control, such as the trade-off between fast responding and accurate stopping, captured complementarily by the go reaction times (goRTs) and the stopping accuracy. This is important, because functional studies show that different rIFG subregions are involved in motor initiation as well as proactive and reactive inhibition (Hartwigsen et al., 2019; Messel et al., 2019). However, the interpretation of goRTs produced under the SST as task-general marker of motor preparation has been challenged. For instance, SST goRTs have been found to slow down with increasing probability of a stop signal (Zandbelt and Vink, 2010), which has been taken as evidence for a braking mechanism that proactively restrains responses (proactive inhibitory control) (Zandbelt and Vink, 2010; Albares et al., 2014). Thus, motor initiation in the SST seems to be influenced by other cognitive mechanisms, such as strategic slowing in order to balance performance speed and accuracy (Leotti and Wager, 2010). Correspondingly, it has been found that activations associated with go responses in the SST overlap with those related to outright stopping (e.g., the preSMA and striatum, Forstmann et al., 2008). It has also been reported that the IFG and preSMA are involved during unconsciously initiated response slowing in tasks other than the SST (van Gaal et al., 2010).

Contrasting the SST with a response choice task represents the ideal tool to study the associations of rIFG subdivisions with respect to their potential involvement in response generation and inhibition. We therefore investigated the associations of rIFG subregions with response initiation (responding without stopping constraints in a pure response choice task), response initiation under proactive inhibitory control (goRT in SST), as well as response inhibition under reactive inhibitory control (stop signal reaction time and accuracy in the SST).

The primary aim of the present study was to map the structural connections of the three subregions of the rIFG: the pars opercularis, pars triangularis and pars orbitalis. Further, we extended the abovementioned literature by investigating the white matter fiber pathways connecting the dorsal and ventral region of the pars opercularis to regions critical for motor control. We expected that the dorsal and ventral connections would show differential functional associations such that connections from the dorsal part would be associated with response initiation irrespective of the task context (that is, we expect associations with the go reaction times both in the response task and in the SST), while those of the ventral part would show associations with measures of response inhibition (i.e., stop signal reaction time).

MATERIALS AND METHODS

Participants

Thirty-one participants took part in the experiment (14 females, mean age = 26.35, range = 20–36 years). One participant was excluded from behavioral and connectivity analyses due to technical issues that caused partial data loss. Five participants were excluded from the behavioral analyses: two participants were excluded due to technical issues with the response device, two more did not complete the behavioral tasks, and one participant was excluded due to an interruption in the middle of the experiment, leading to non-convergence of the stop signal delays (SSD). This resulted in 30 participants for the structural connectivity analyses and 25 participants for the analysis of brain-behavior associations. All participants were right-handed, had normal or corrected to normal vision and reported no history of psychiatric or neurological disorders, migraine, or loss of consciousness. The experiment was approved by the internal review board of the Department of Psychology, University of Oslo. All participants gave informed consent and received a gift card of 300 NOK for participation.

Image Acquisition

All magnetic resonance imaging (MRI) sequences were run on a 3.0 Tesla Philips Ingenia whole-body scanner (Philips Medical Systems, Best, Netherlands) with a 32-channel head coil. Diffusion-weighted imaging (DWI) was performed using a single-shot EPI sequence, one b0 image, and diffusion weighting was conducted across 32 non-collinear directions with a b-value = 1000 s/mm^2, flip angle = 90°, repetition time (TR) = 13.45 s, echo time (TE) = 62 ms, field of view (FOV) = 224 × 224 × 120, Matrix = 96 × 94 × 60. The acquired voxels of size 2.33 mm × 2.38 mm × 2.0 mm were reconstructed to 2.0 mm isotropic voxels. T1 images were acquired using the following parameters: TE = 2.3, TR = 5.1, FOV = 256 × 256 × 184, Matrix = 256 × 254 × 184, voxel size = 1.0 mm × 1.0 mm × 1.0 mm.

Data Processing

All processing and transformation steps were conducted in ExploreDTI v.4.8.6 (Leemans et al., 2009). All images were inspected for artifacts and excessive head movements, corrected

for eddy current-induced distortions and head motions with a non-diffusion weighted image as reference. Plugin options for artifact correction in ExploreDTI were used, including one for EPI correction (Leemans and Jones, 2009; Irfanoglu et al., 2012). Specifically, as part of the initial quality assessment, all diffusion-weighted images were loaded to ExploreDTI and looped for each subject using the "loop" function in the "QA DWIs" tool. For the automatic processing steps, we utilized each participant's high-resolution T1-weighted image to cope with distortions induced during DWI. Here, all corrections were included in one interpolation step (i.e., subject motion and echo current induced distortions), in which the T1 image was used to unwarp deformations. To further improve the correction procedure, the registration was constrained along the phase encoding direction. Tensor estimation was performed using a linear estimation approach, which is the default estimation approach in the ExploreDTI toolbox (Tax et al., 2015). Finally, the diffusion weighted images were aligned with the T1 image, and correspondingly resampled to 1mm isotropic voxels, and overlayed with the T1 image for final inspection of the outputs (see **Supplementary Figure 1** for sample participant).

Brain Atlas and Tractography

A standardized brain atlas consisting of the Automated Anatomical Labeling (AAL) atlas (Tzourio-Mazoyer et al., 2002) and a bilateral binarized mask of the STN (Forstmann et al., 2012) were used to outline 92 brain regions across both hemispheres. The AAL atlas does not separate the preSMA and SMA proper region, and there are short frontal tracts that connects the IFG to both the preSMA and SMA proper region (Catani et al., 2012), without a clear separation between the two regions. Thus, we further used the AAL region for the SMA to increase the reliability of the tracts across participants to prevent the possibility for the same tract ending in the preSMA region in some participant, while in the SMA proper in other participants (potentially at the expense of decreased regional specificity of the connections). Here, the preSMA and SMA proper will collectively make up a region that will be referred to as SMA complex (SMAc). Further, a whole brain deterministic tractography with every voxel as seed point was completed with the following parameters: seed point resolution = 1 mm isotropic and angle threshold = 45°, FA threshold = 0.2, fiber length range = 50–500 mm, step size = 1. The "From atlas template/labels" tool in ExploreDTI was used to register an atlas template to the corrected data for each participant, which resulted in 92*92 connectivity matrices for every participant. From these connectivity matrices, the passing and ending tracts of the three subregions of the rIFG were extracted. An ending connection was determined between two regions if the reconstructed fiber pathway originated in one of the regions and terminated in the other (i.e., the "END" option in ExploreDTI). A connection was deemed a passing pathway if the reconstructed tract passed through the regions (i.e., the "PASS" option in ExploreDTI). We reran the same procedure after parcelating the pars opercularis into a dorsal and ventral region based on a halfway split along its longest extent. Specifically, a new connectivity matrix was created including the parcelated dorsal and ventral pars opercularis,

as well as the regions of interest that had previously shown reconstructed connections with the right pars opercularis. Then, we extracted the connectivity profile seeding from the dorsal and ventral part of the pars opercularis, respectively. It is important to note that the results derived from the connectivity matrices should not be interpreted as true measure of fiber pathways in the brain, but are reconstructed streamlines from the deterministic tractography procedure (henceforth referred to as reconstructed connections).

Tasks and Procedure

All participants were measured on two separate days (with a median interval of 1 day). Session one consisted of three MRI sequences, including a T1, DWI and resting-state fMRI measurement. Session two consisted of a concurrent measurement of electroencephalography (EEG), single-pulse transcranial magnetic stimulation (TMS), and electromyography (EMG) during two separate computer-based experiments: the delayed response task (DRT) and the stop signal task (SST). As this study focused on the associations of white-matter structure with behavior, the acquired EEG, EMG, and TMS data will not further be regarded here.

The experimental tasks were developed as in-house MATLAB scripts (The MathWorks, Inc., Massachusetts, United States) using the Psychophysics Toolbox (Brainard, 1997; Pelli, 1997; Kleiner et al., 2007). Participants sat in a chair at a viewing distance of 1 m from the monitor and responded on separate response devices with their left and right index fingers. The screen resolution was 1280*1024 with a refresh rate of 60 Hz. The experimental tasks consisted of a cued DRT of 3 blocks and a cued SST of 12 blocks. Each block took approximately 6 min to complete with the possibility to take breaks of self-determined durations in-between each block and task (total time = 92,4 min + pauses). Trials containing TMS pulses were excluded from the analyses. The DRT data consisted of 96 non-TMS pulse trials with 72 go-trials and 24 catch trials, while the SST consisted of 432 non-TMS pulse trials with 288 go-trials and 144 stop trials. The go and stop stimuli were presented as circles colored either blue or orange. The colors of the stimuli were counterbalanced for the go and stop signal; the color of the go signal remained the same for the DRT and SST throughout the experiment.

The cued DRT started with a fixation cross randomly jittered between 1,800 and 2,300 ms. After this, a cue (i.e., a right or left leaning bracket) was presented that indicated which finger to prepare for a response (e.g., right leaning bracket = right index finger). The inclusion of these valid cues eliminated the decision making phase after the detection of the go signal (as the decision about which hand to use is shifted to the cue-delay period), and thus allows for the investigation of response initiation without confounding response conflict. The cue duration was fixed at 900 ms. The go signal (a circle next to the bracket) appeared after the cue and was present for 800 ms or until a response was made. A go signal was omitted in 9% of the trials to diminish premature responding. The SST was similar in all aspects of the task but two: (i) the inclusion of a stop signal in a minority of the trials, and (ii) that no go signals were omitted. Stop signals appeared

in 33% of the trials and were presented after a stop signal delay (SSD) that was adjusted following a tracking procedure. The SSD was initially set to 250 ms for both hands and was subsequently adjusted based on the performance in the preceding trial. The SSD was increased by 33 ms if the previous stop signal trial was successful, and decreased by 33 ms after unsuccessful stop trials. The minimum and maximum SSD were set to 80 and 800 ms, respectively. All stimuli included in the tasks were visual, including the stop signal in the SST.

Instructions

For the DRT, participants were told to respond as fast as possible to the circle appearing next to the cue. For the SST, the participants were told that the task was similar to the DRT, but that a stop signal would be shown on a minority of the trials to which they should try to withhold their response. They were further instructed to be as fast and accurate as possible and that mistakes were to be expected during the task. In go trials, feedback ("too late") was presented if no response was produced within 800 ms after the go signal. The participants were also shown feedback after each block. If the average goRT of the preceding block was above 600 ms, the participants were instructed to be faster. However, if the average accuracy was below 45%, they were instructed to be more accurate. If the participants' performance was within these thresholds, they were presented with the feedback "Well done."

Derivation of Dependent Variables and Statistical Analyses

To quantify white matter microstructure, we extracted the FA values of the tracts of interest from the whole brain tractography analyses. Further, the average FA across the brain for each participant was derived by calculating the mean value of the FA for all passing and ending tracts across the brain and averaging these into a single global FA value. Specifically, this was derived from the FA values across the reconstructed connections corresponding to the 92*92 connectivity matrices (only cortical and subcortical regions as per the AAL atlas described above). Two regions were deemed connected if it showed any number of streamlines between the two regions. To test if the rIFG subregions differed in their number of binary connections to other brain regions, we ran paired t-tests between the total number of binary connections each subregion exhibited for each participant. Here, we define the number of interconnected regions as node degree, or more specifically the out-degree (the number of out-going edges or connections, differentiating for passing and terminating tracts) Thus, the paired t-tests include the node degree for each of the three rIFG subregions to test differences between the number of interconnected regions. Note that this was derived from a connectivity matrix that only included real value entries if a tract was identified during tractography with the parameters outlined above, with zeros for the regions for which tracts could not be identified. This allowed us to quantify the number of cortical regions that were connected to each rIFG subregion by simply counting the non-zero entries for each participant. As false positives and false negatives could

influence reconstructed brain networks (de Reus and van den Heuvel, 2013), we also confirmed the results from the paired t-test after using a group detection threshold (i.e., only including the binary connections that were present in at least 80% of the individuals). The results from the paired t-tests using the 80% detection threshold can be found in **Supplementary Note 2**.

The following behavioral measures were extracted from the DRT and SST: Go-accuracy, goRT, probability of choice errors, omissions, and premature responses (responses given after the cue, but before go signal onset). For the SST, we also calculated the stopping accuracy, unsuccessful stop RT, stop signal delay, and stop signal reaction time (SSRT). The SSRTs were estimated based on the integration method (Verbruggen and Logan, 2009). Specifically, the goRT distribution for each participant was extracted that included premature responses and go errors, and the omissions were replaced by the maximum go RT (Verbruggen et al., 2019). The SSRT was calculated by subtracting the mean SSD from the n_{th} value in the sorted goRT distribution, where n corresponds to the probability of responding in the stop trials multiplied with the number of values in the go RT distribution. All behavioral measures are reported as an average of both hands. The association between the goRT and SSRT in the SST was calculated as a parametric bivariate correlation. All statistical analyses assessing behavioral and brain-behavior associations were carried out with IBM SPSS Statistics for Windows, Version 25.0.
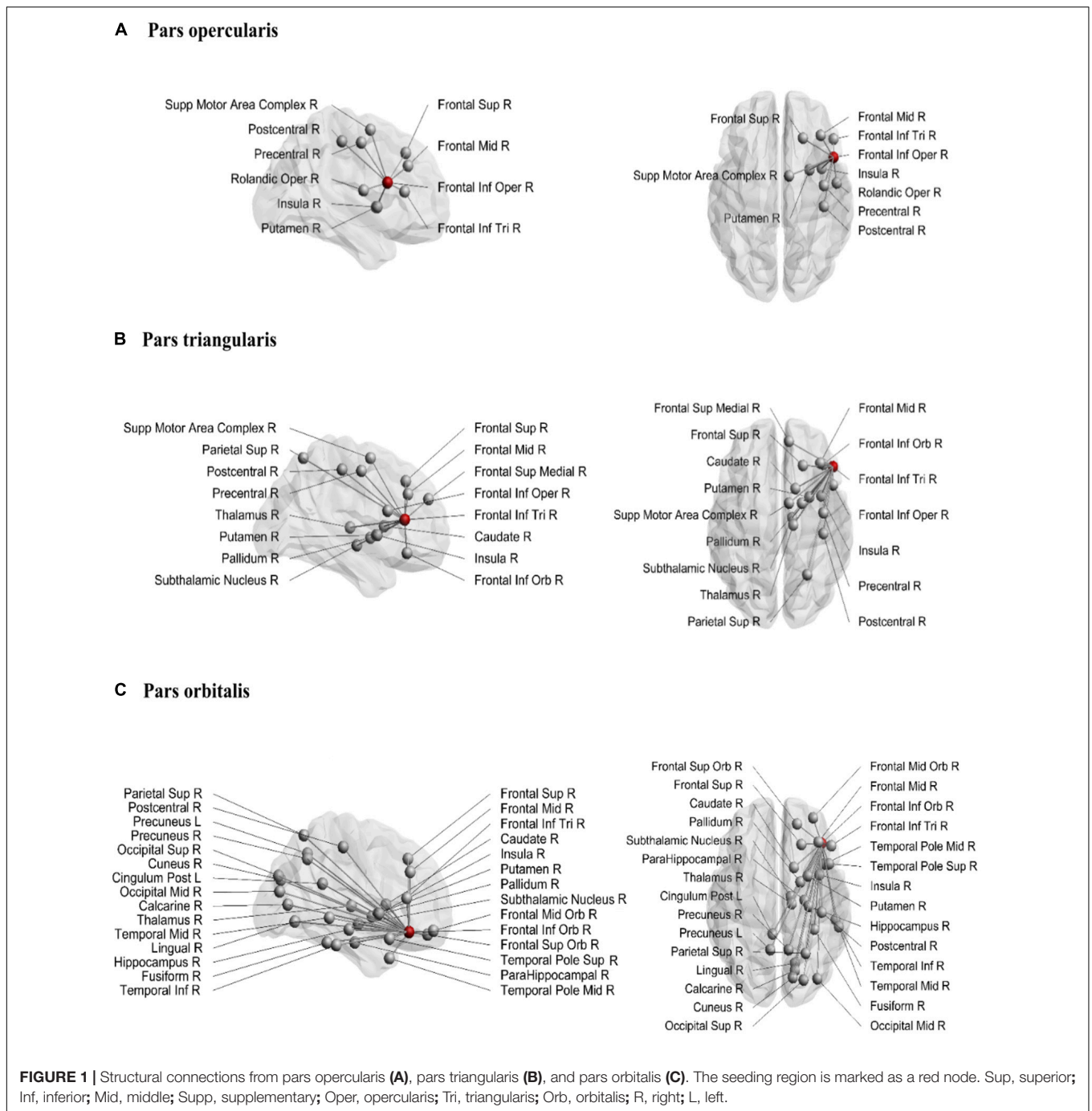
Brain-Behavior Analyses

The goRT, SSRT, and stopping accuracy were used as dependent variables, and the global FA and parameters of the tracts from the dorsal and ventral part of the pars opercularis and to the target region SMAc were used as predictor variables in the regression analyses. First, the global FA may be associated with general cognitive ability, thus we expected correlations with all of the behavioral measures (i.e., DRT and SST goRT, SSRT, and stopping accuracy). For this reason, the global FA was also included in the regression analyses to account for global inter-individual differences in white matter microstructure of the brain. We specifically focused on the pars opercularis as it has been considered the key node of inhibitory control (Aron et al., 2014; Hartwigsen et al., 2019). For visualizations and brain-behavior analyses, we used tracts that were present in at least 80% of the participants for generalizability and reliability.
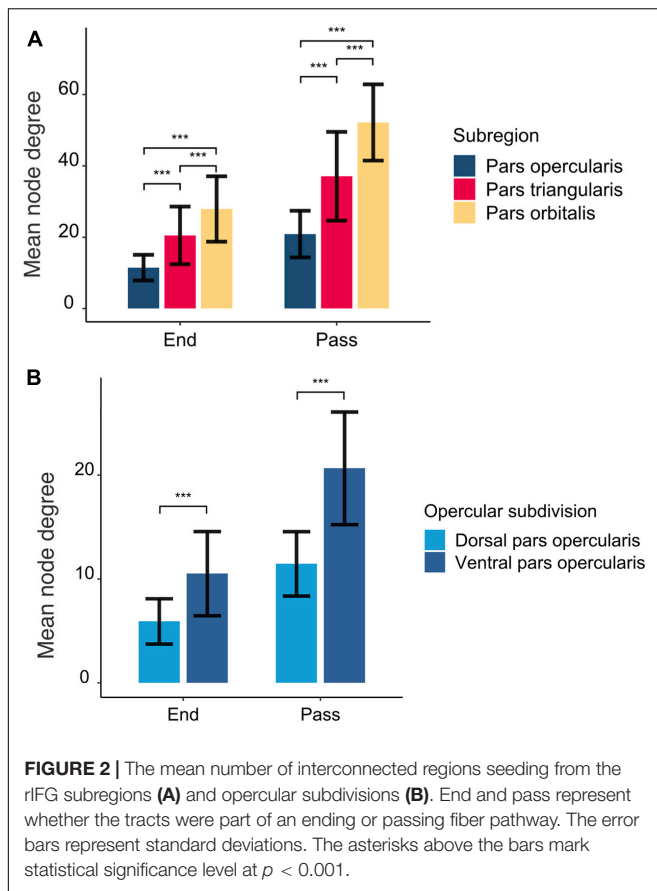
RESULTS

Structural Connectivity Maps of the Three Right Inferior Frontal Gyrus Subregions

The structural connections of the rIFG sub-regions are visualized in **Figure 1**, and the mean node degree of passing and ending tracts for each subregion is depicted in **Figure 2**. In total, the three subregions showed extensive inter-regional connectivity that covered all four lobes in the right hemisphere, as well as several structures within the basal ganglia. The pars

FIGURE 1 | Structural connections from pars opercularis **(A)**, pars triangularis **(B)**, and pars orbitalis **(C)**. The seeding region is marked as a red node. Sup, superior; Inf, inferior; Mid, middle; Supp, supplementary; Oper, opercularis; Tri, triangularis; Orb, orbitalis; R, right; L, left.

opercularis (**Figure 1A**) exhibited a similar connectivity pattern as the pars triangularis, albeit with fewer interconnected regions (**Figure 1B**), while the connectivity fingerprint of the pars orbitalis (**Figure 1C**) exhibited a more widespread network that also reached peripheral regions such as the occipital cortex (see **Supplementary Figure 2** for a sample participant). The data may suggest a posterior to anterior gradient with increasing connectivity from the opercularis, via the triangularis, to the orbitalis. To quantitatively test this observation, we computed pair-wise t-tests between these regions with the node degree

estimated for each subject as dependent variable (**Figure 2**). These tests were run separately for both passing and terminating projections. For the terminating reconstructed connections, the results revealed a significantly lower node degree for the pars opercularis compared to the pars triangularis [$t(29) = -6.67$, $p < 0.001$] and the pars orbitalis [$t(29) = -9.04$, $p < 0.001$], while the pars triangularis showed a lower node degree compared to the pars orbitalis [$t(29) = -3.98$, $p < 0.001$]. A similar pattern emerged for passing connections, where the pars opercularis exhibited a lower node degree compared to the pars triangularis

FIGURE 2 | The mean number of interconnected regions seeding from the rIFG subregions **(A)** and opercular subdivisions **(B)**. End and pass represent whether the tracts were part of an ending or passing fiber pathway. The error bars represent standard deviations. The asterisks above the bars mark statistical significance level at $p < 0.001$.

$[t(29) = -8.46, p < 0.001]$ and the pars orbitalis $[t(29) = -14.38, p < 0.001]$, while the pars triangularis showed a lower node degree compared to the pars orbitalis $[t(29) = -6.59, p < 0.001]$.

Structural Connectivity Maps of the Dorsal and Ventral Pars Opercularis

The structural connections of the dorsal and ventral pars opercularis are visually presented in **Figure 3**. While the connectivity patterns of these two subregions show considerable overlap, the ventral part of the pars opercularis exhibited a higher node degree as indicated via significant paired t-tests for both ending $[t(29) = -6.49, p < 0.001]$ and passing $[t(29) = -9.20, p < 0.001]$ tracts. Connectivity differences emerged such that the dorsal opercularis showed a connection to mid-frontal cortex, whereas the ventral opercularis showed connections to postcentral cortex, rolandic operculum, insula, and putamen.

IFG Connectivity Within the Stopping Network

We conducted a connectivity analysis that specifically focused on differential connectivity patterns of the three IFG subregions with the other brain areas considered part of the stopping network: the SMAc, insula, caudate, putamen, and the STN. Connections to the stopping network were deemed to be reliably present if they were identified in at least 80% of the participants. **Figure 4** depicts

the frequencies of these connections and **Figure 5** depicts the connections. The pars opercularis showed reliable connections to the SMAc, insula, and putamen. The pars triangularis showed reliable connections to the SMAc, insula, putamen, caudate, and the STN. The pars orbitalis exhibited reliable connections to the insula, putamen, caudate, and STN. Thus, the three rIFG subregions showed a differential connectivity within the stopping network, with connectivity in pars opercularis being limited to the cortical areas and putamen, while the other two regions showed additional subcortical basal ganglia connections.
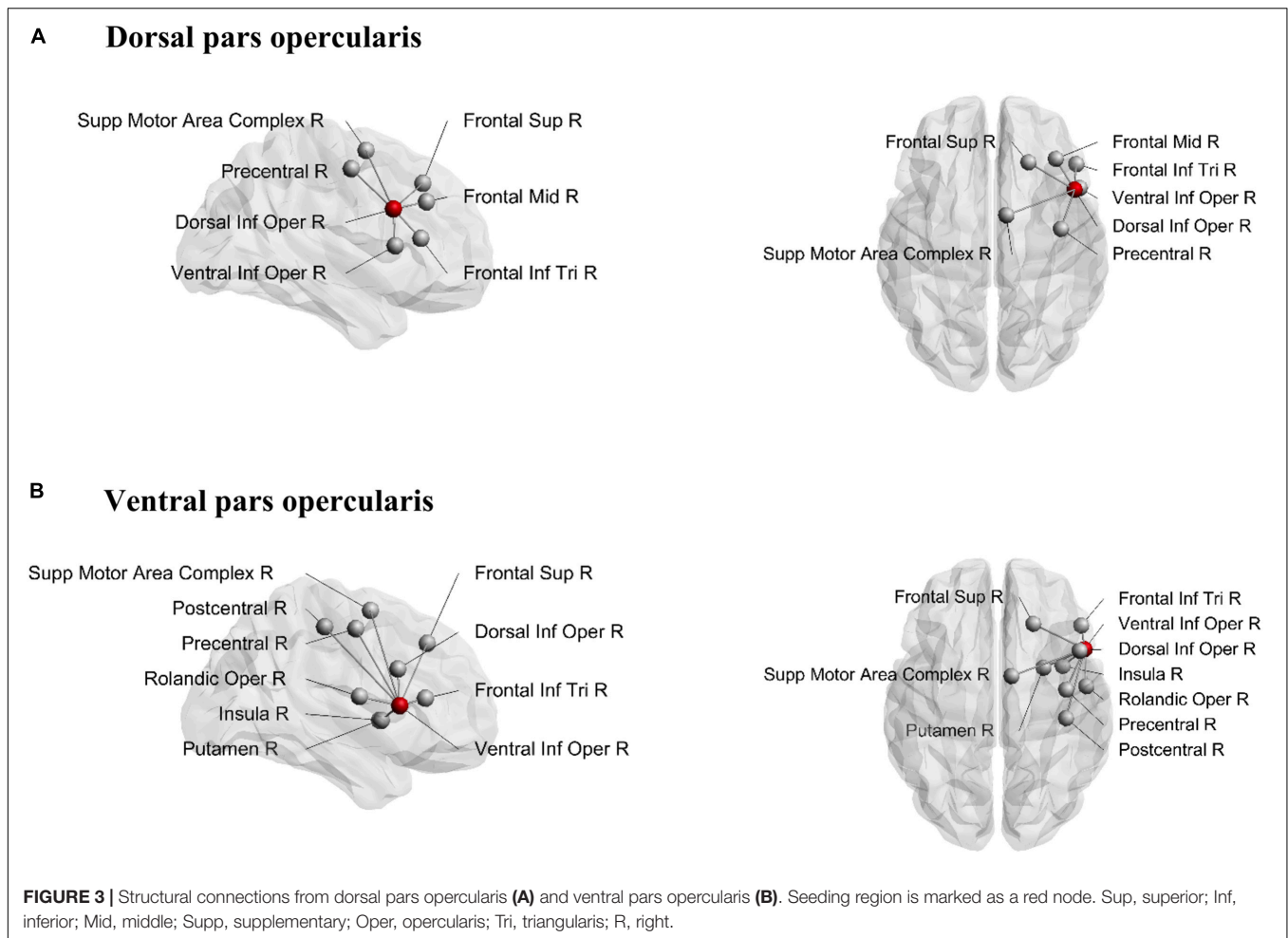
Behavioral Results

Descriptive statistics of the behavioral measures obtained from the DRT and SST are presented in **Table 1**. Across participants, the average accuracy ($\geq$ 95% in both tasks) indicated good task performance. The average stop accuracy was 48%, which indicated successful SSD tracking, and all participants showed faster unsuccessful stop RTs than go RTs. The goRTs were shorter in the DRT than in the SST $[t(24) = -9.18, p < 0.001]$ and did not correlate with each other ($r = 0.081, p = 0.700$). The average SSRT was 209 ms and did not correlate significantly with the mean goRT in the SST ($r = -0.30, p = 0.15$). However, stopping accuracy showed a significant association with goRT ($r = 0.57, p = 0.003$) and SSRT ($r = -0.60, p < 0.001$) in the SST.

Global and Tract-Specific Associations With Behavior

First, we tested whether the global FA was predictive of task performance, and found that the global FA value was not significantly correlated with the DRT goRT ($r = 0.091, p = 0.664$), but that it exhibited significant correlations with the SST goRT ($r = 0.434, p = 0.030$), SSRT ($r = -0.414, p = 0.040$) and stopping accuracy ($r = 0.479, p = 0.015$). Note that under conservative control for Type I error, these correlations would not survive correction for multiple comparisons in our sample. However, we consider the effect sizes and the consistencies across different behavioral measures sufficient to warrant the inclusion of the global FA in the regression models.

We then focused more specifically on key regions of the stopping network. Given the putative interactions of the pars opercularis and the SMAc in the stopping literature and their role in motor and inhibitory control, we computed a linear regression analysis using the FA of the dorsal pars opercularis-SMAc and the ventral pars opercularis-SMAc tracts as predictors of DRT goRT, SST goRT, SSRT, and stopping accuracy (**Table 2**). The global FA was added as a covariate, given the aforementioned associations of global FA with task performance measure, to further test the regional specificity of the described effects. The full model was only significant for the SST goRT and accuracy with the dorsal pars opercularis-SMAc tract as a significant predictor. The associations were also found to be significant with age and sex included as covariate instead of the global FA value (**Supplementary Note 1**). **Figure 6** depicts the associations between the goRT in the DRT and the SST and stopping accuracy with the dOp-SMAc tract.

FIGURE 3 | Structural connections from dorsal pars opercularis **(A)** and ventral pars opercularis **(B)**. Seeding region is marked as a red node. Sup, superior; Inf, inferior; Mid, middle; Supp, supplementary; Oper, opercularis; Tri, triangularis; R, right.

DISCUSSION

Our primary objective was to investigate the white matter fiber pathways of three rIFG sub-regions (i.e., pars opercularis, pars triangularis, and pars orbitalis) using diffusion weighted imaging and deterministic tractography. The three subregions showed substantial differences in their connectivity patterns, as well as

FIGURE 4 | Histogram illustrating the percentage of participants having connections from the rIFG subregions to the regions within the stopping network. The vertical dashed line refers to the inclusion threshold of 80% for a reliable connection. SMAc, supplementary motor area complex; STN, subthalamic nucleus.

a posterior to anterior gradient in node degrees. In addition, the pars opercularis was segmented into a dorsal and ventral region, both of which were shown to have connections to SMAc. However, only the fractional anisotropy of the dOp-SMAc tract was a significant predictor of task behavior, namely for the goRT and stopping accuracy in the SST.

Hartwigsen et al. (2019) identified functionally diverse subregions in the rIFG, following a posterior-to-anterior axis, where the posterior part was associated with motor functioning and the anterior part was related to abstract cognitive functions. In relation to this, we found evidence for a posterior-to-anterior division of structural connections within the rIFG. That is, the pars orbitalis showed the highest number of interconnected regions, followed by the pars triangularis, while the pars opercularis exhibited the lowest number of interconnected regions. Moreover, the connectivity fingerprints of the pars opercularis and pars triangularis were largely restricted to central and frontal regions, while the pars orbitalis showed the most widespread inter-regional connectivity pattern among the three rIFG sub-regions. This is interesting as the pars orbitalis has been associated with abstract cognitive functions (Hartwigsen et al., 2019), whereas the current study indicates that it also shows a widespread connectivity pattern reaching regions across all four
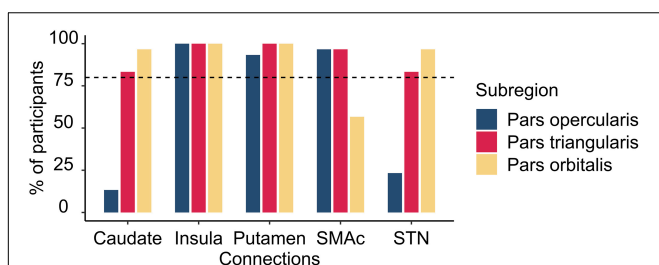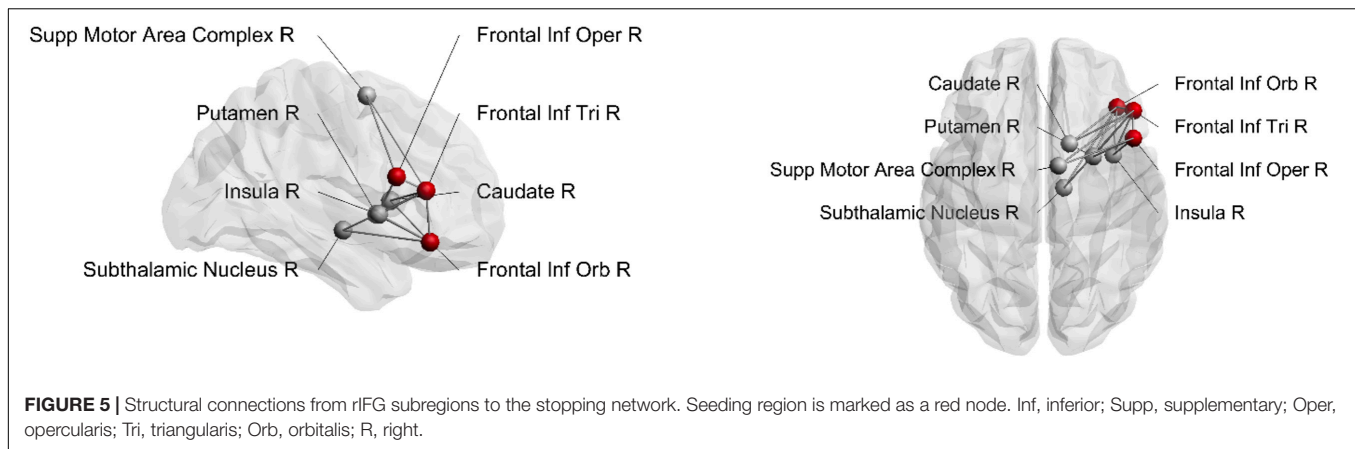
FIGURE 5 | Structural connections from rIFG subregions to the stopping network. Seeding region is marked as a red node. Inf, inferior; Supp, supplementary; Oper, opercularis; Tri, triangularis; Orb, orbitalis; R, right.

lobes in the right hemisphere. Speculatively, it might be that the widespread connections of the pars orbitalis serve its involvement in complex cognitive functioning, such as abstract thinking and social cognition. This is in contrast to the posterior part of the rIFG, which has been proposed to be crucial for inhibitory control (Aron et al., 2014), with a further subdivision of a dorsal region involved in motor execution and a ventral region involved in motor inhibition (Hartwigsen et al., 2019). In the current study, the segmentation of the pars opercularis into a dorsal and ventral region revealed some marked differences where the ventral part of the pars opercularis showed a higher inter-regional connectivity compared to the dorsal part. In addition, both regions exhibited connections to the SMAc, an important region within the stopping network. Altogether, in line with previous evidence suggesting a functional divergence in the rIFG along its posterior-to-anterior axis, our results showed increased node degrees along the posterior-to-anterior axis as well, possibly reflecting a structurally diverse rIFG.

We also identified several connections of the rIFG sub-regions to other parts of the stopping network. The pars opercularis showed reliable connections to the SMAc, insula, and putamen. Surprisingly, we did not find evidence for a reliable connection from the pars opercularis to the STN. This is in contrast to previous research that has shown this connection

(Isaacs et al., 2018), albeit with data acquired with ultra-high field MRI and probabilistic tractography. However, the current results do show a reliable connection from both the pars triangularis and pars orbitalis to the STN. This might indicate that a connection between the pars opercularis and the STN consists of a tract with a complex architecture, which is harder to reconstruct with the conservative tractography technique used in the present study. It is interesting to note, however, that the pars triangularis was the only rIFG subregion that showed

TABLE 1 | Behavioral characteristics.

	DRT	SST
Go accuracy, %	96 (3.92)	95 (2.7)
Choice errors, %	0.38 (0.74)	0.24 (0.34)
Go omissions, %	1.48 (1.73)	3.15 (1.62)
Premature responses, %	1.89 (3.35)	1.21 (1.68)
Go RT, ms	320 (53)	475 (70)
Stop accuracy, %	–	48 (3.83)
Unsuccessful stop RT, ms	–	409 (74)
Stop signal delay, ms	–	293 (91)
Stop signal reaction time, ms	–	209 (26)

Go RT, mean reaction time on go trials; ms, milliseconds, standard deviations are presented in the brackets.

TABLE 2 | Summary of multiple regression analyses ($N = 20$).

	B	SE B	β	t	P
SST go reaction time ($R^2 = 0.485$, adjusted $R^2 = 0.394$, $F = 5.336$, $p = 0.009$)					
Intercept	−658.553	436.643		−1.508	0.150
Global FA	2142.835	1170.607	0.372	1.831	0.085
dOp-SMAc	2150.711	810.318	0.793	2.654	0.017
vOp-SMAc	−1568.957	875.468	−0.527	−1.792	0.091
SST stop signal reaction time ($R^2 = 0.221$, adjusted $R^2 = 0.084$, $F = 1.611$, $p = 0.224$)					
Intercept	537.138	209.253		2.567	0.020
Global FA	−575.825	560.993	−0.257	−1.026	0.319
dOp-SMAc	−487.667	388.331	−0.461	−1.256	0.226
vOp-SMAc	273.082	419.553	0.235	0.651	0.524
SST stop accuracy,% ($R^2 = 0.495$, adjusted $R^2 = 0.405$, $F = 5.547$, $p = 0.008$)					
Intercept	−20.243	26.058		−0.777	0.448
Global FA	111.247	69.860	0.321	1.592	0.130
dOp-SMAc	128.572	48.359	0.787	2.659	0.017
vOp-SMAc	−75.158	52.247	−0.419	−1.439	0.168
DRT go reaction time ($R^2 = 0.037$, adjusted $R^2 = −0.133$, $F = 0.217$, $p = 0.883$)					
Intercept	176.723	528.020		0.335	0.742
Global FA	458.469	1415.582	0.090	0.324	0.750
dOp-SMAc	623.966	979.895	0.260	0.637	0.533
vOp-SMAc	−732.951	1058.679	−0.278	−0.692	0.498

SST, stop signal task; DRT, delayed response task; dOp, dorsal pars opercularis; vOp, ventral pars opercularis; SMAc, supplementary motor area complex. All predictors had tolerance > 0.1 and variation inflation factor < 0.3.
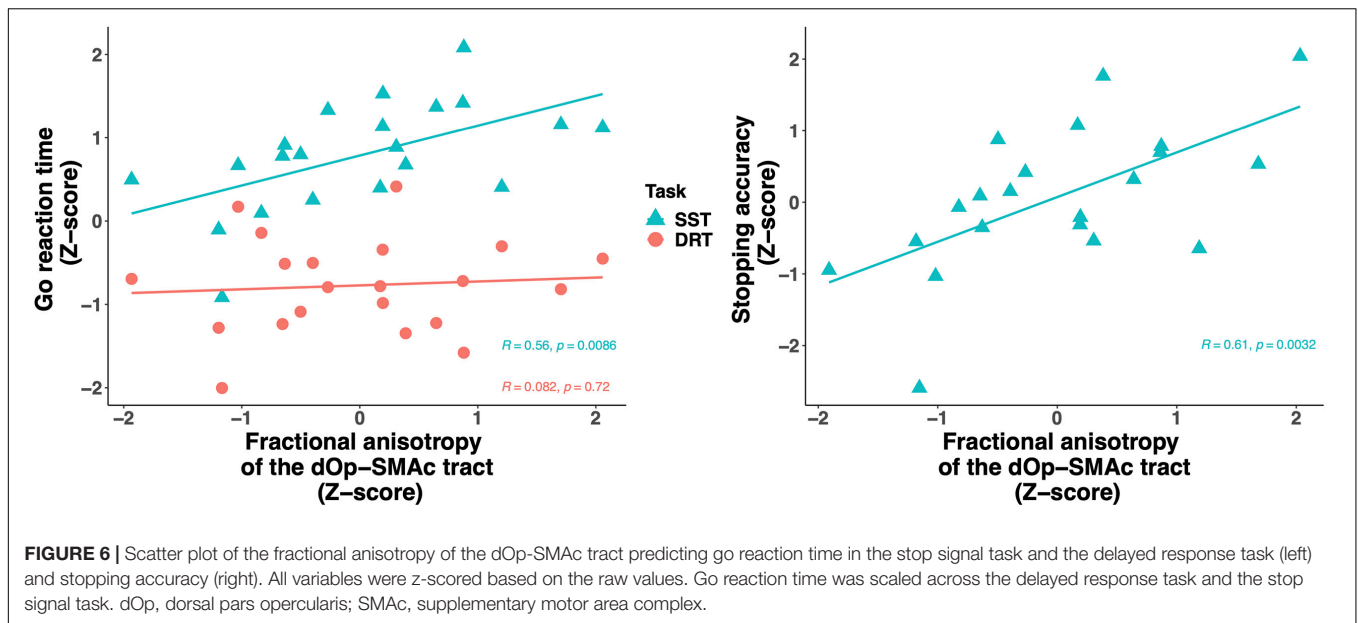
FIGURE 6 | Scatter plot of the fractional anisotropy of the dOp-SMAc tract predicting go reaction time in the stop signal task and the delayed response task (left) and stopping accuracy (right). All variables were z-scored based on the raw values. Go reaction time was scaled across the delayed response task and the stop signal task. dOp, dorsal pars opercularis; SMAc, supplementary motor area complex.

a reliable connection to the SMAc, insula, putamen, caudate and STN. Given the overlapping connectivity fingerprints of the pars opercularis and pars triangularis, the combination of these regions might be a more suitable connectivity hub for inhibitory control compared to pars opercularis alone. Altogether, the results show connections between rIFG subregions and other regions that were also found in a meta-analysis on functional MRI during inhibitory control, and which included the insula, SMAc, middle frontal gyrus, striatum, and posterior parietal area (Cai et al., 2019).

Furthermore, Hartwigsen et al. (2019) suggested that the posterior part of the rIFG could be segmented into a dorsal and ventral region and that these regions are associated with motor initiation and inhibition, respectively. However, it is unclear whether the dorsal part relates to the cognitive effort necessary to execute correct responses in demanding tasks, or whether it relates to motor execution proper. In the current study, both the dorsal and ventral regions of the pars opercuarlis showed connections to the SMAc, a connection that has been suggested to be important for inhibitory control (Aron et al., 2007; Swann et al., 2012). Thus, it is interesting that our results revealed a significant positive relationship between the dorsal pars opercularis-SMAc and the goRT from the SST, while the ventral pars opercularis-SMAc showed a (non-significant but considerable) negative relationship with the goRT. We also observed the same pattern for the stopping accuracy, showing that increased connectivity strength in the dorsal pars opercularis-SMAc is related to increased reaction time and stopping accuracy. This is interesting in context of previous research that showed increased fractional anisotropy in the pars opercularis to be negatively associated with the SSRT, while increased fractional anisotropy in the preSMA was positively associated with the SSRT (Xu et al., 2016). Moreover, the dorsal pars opercularis-SMAc tract was a significant predictor of goRT in the SST and not the DRT, and the goRTs from the DRT and

SST did not correlate. This suggests that the goRTs obtained from the SST are influenced by other cognitive control mechanisms than motor generation alone. This supports a role of the dorsal opercularis in cognitively demanding motor initiation or the balancing of response speed and accuracy as opposed to plain motor generation in itself. The observed pattern thus supports the hypothesis of different functional roles of the dorsal and ventral parts of the opercularis.

In conclusion, the results indicate that the three sub-regions of the rIFG exhibit heterogeneity in terms of their connectivity, which is supported by the difference in the intra and inter-individual amount of tracts across the sub-regions. The overall pattern followed a posterior to anterior gradient with increasing node degrees from the pars opercularis, via the pars triangularis and to the pars orbitalis. Although, the pars orbitalis showed the most widespread connectivity, all three rIFG subregions showed several connections to regions implicated in inhibitory control. The segmentation of the dorsal and ventral pars opercularis showed that both regions had reliable connections to the SMAc, but only the ventral part was connected to the insula and putamen. We believe that the results from the current study provide novel insights into connectivity differences between the rIFG subregions. As always, some caution is warranted as quantitative differences in streamlines can also be caused by other microstructural differences (e.g., branching, length, and curvature of tracts; Jones et al., 2013). Finally, the go reaction times from the SST were considerably longer compared to that of the DRT, likely due to demand for increased cognitive control. Thus, associations between measures of motor initiation in a more cognitive demanding task (i.e., reaction time in the SST) and brain structure may reflect multiple aspects of action generation, including motor preparation, uncertainty estimation, and movement invigoration. Taken together, the brain-behavior associations partly supported a functional differentiation between the dorsal and ventral pars opercularis, possibly implicating them

in response execution under increased cognitive control and inhibition, respectively.

DATA AVAILABILITY STATEMENT

The raw data supporting the conclusions of this article will be made available by the authors, without undue reservation.

ETHICS STATEMENT

The study was reviewed and approved by the Internal Review Board of the Department of Psychology, University of Oslo.

The participants provided their written informed consent to participate in this study.

AUTHOR CONTRIBUTIONS

SUPPLEMENTARY MATERIAL

The Supplementary Material for this article can be found online at: https://www.frontiersin.org/articles/10.3389/fnhum. 2022.787079/full#supplementary-material

REFERENCES

Albares, M., Lio, G., Criaud, M., Anton, J.-L., Desmurget, M., and Boulinguez, P. (2014). The dorsal medial frontal cortex mediates automatic motor inhibition in uncertain contexts: evidence from combined fMRI and EEG studies. *Hum. Brain Mapp.* 35, 5517–5531. doi: 10.1002/hbm.22567

Aron, A. R., Behrens, T. E., Smith, S., Frank, M. J., and Poldrack, R. A. (2007). Triangulating a Cognitive Control Network Using Diffusion-Weighted Magnetic Resonance Imaging (MRI) and Functional MRI. *J. Neurosci.* 27, 3743–3752. doi: 10.1523/JNEUROSCI.0519-07.2007

Aron, A. R., Herz, D. M., Brown, P., Forstmann, B. U., and Zaghloul, K. (2016). Frontosubthalamic Circuits for Control of Action and Cognition. *J. Neurosci.* 36, 11489–11495. doi: 10.1523/JNEUROSCI.2348-16.2016

Aron, A. R., Robbins, T. W., and Poldrack, R. A. (2014). Inhibition and the right inferior frontal cortex: one decade on. *Trends Cogn. Sci.* 18, 177–185. doi: 10.1016/j.tics.2013.12.003

Brainard, D. H. (1997). The Psychophysics Toolbox. *Spat. Vis.* 10, 433–436. doi: 10.1163/156856897X00357

Cai, W., Duberg, K., Padmanabhan, A., Rehert, R., Bradley, T., Carrion, V., et al. (2019). Hyperdirect insula-basal-ganglia pathway and adult-like maturity of global brain responses predict inhibitory control in children. *Nat. Commun.* 10:4798. doi: 10.1038/s41467-019-12756-8

Catani, M., Dell'Acqua, F., Vergani, F., Malik, F., Hodge, H., Roy, P., et al. (2012). Short frontal lobe connections of the human brain. *Cortex* 48, 273–291. doi: 10.1016/j.cortex.2011.12.001

Chambers, C. D., Garavan, H., and Bellgrove, M. A. (2009). Insights into the neural basis of response inhibition from cognitive and clinical neuroscience. *Neurosci. Biobehav. Rev.* 33, 631–646. doi: 10.1016/j.neubiorev.2008. 08.016

de Reus, M. A., and van den Heuvel, M. P. (2013). Estimating false positives and negatives in brain networks. *NeuroImage* 70, 402–409. doi: 10.1016/j. neuroimage.2012.12.066

Forstmann, B. U., Dutilh, G., Brown, S., Neumann, J., von Cramon, D. Y., Ridderinkhof, K. R., et al. (2008). Striatum and pre-SMA facilitate decision-making under time pressure. *Proc. Natl. Acad. Sci. U. S. A.* 105, 17538–17542. doi: 10.1073/pnas.0805903105

Forstmann, B. U., Keuken, M. C., Jahfari, S., Bazin, P.-L., Neumann, J., Schäfer, A., et al. (2012). Cortico-subthalamic white matter tract strength predicts interindividual efficacy in stopping a motor response. *NeuroImage* 60, 370–375. doi: 10.1016/j.neuroimage.2011.12.044

Hartwigsen, G., Neef, N. E., Camilleri, J. A., Margulies, D. S., and Eickhoff, S. B. (2019). Functional Segregation of the Right Inferior Frontal Gyrus: evidence From Coactivation-Based Parcellation. *Cereb. Cortex* 29, 1532–1546. doi: 10. 1093/cercor/bhy049

Irfanoglu, M. O., Walker, L., Sarlls, J., Marenco, S., and Pierpaoli, C. (2012). Effects of image distortions originating from susceptibility variations and concomitant fields on diffusion MRI tractography results. *NeuroImage* 61, 275–288. doi: 10.1016/j.neuroimage.2012.02.054

Isaacs, B. R., Forstmann, B. U., Temel, Y., and Keuken, M. C. (2018). The Connectivity Fingerprint of the Human Frontal Cortex, Subthalamic Nucleus, and Striatum. *Front. Neuroanat.* 12:60. doi: 10.3389/fnana.2018. 00060

Jahanshahi, M., Obeso, I., Rothwell, J. C., and Obeso, J. A. (2015). A fronto–striato–subthalamic–pallidal network for goal-directed and habitual inhibition. *Nat. Rev. Neurosci.* 16, 719–732. doi: 10.1038/nrn4038

Johansen-Berg, H. (2010). Behavioural relevance of variation in white matter microstructure. *Curr. Opin. Neurol.* 23, 351–358. doi: 10.1097/WCO. 0b013e32833b7631

Jones, D. K., Knösche, T. R., and Turner, R. (2013). White matter integrity, fiber count, and other fallacies: the do's and don'ts of diffusion MRI. *NeuroImage* 73, 239–254. doi: 10.1016/j.neuroimage.2012.06.081

Kleiner, M., Brainard, D., Pelli, D., Ingling, A., Murray, R., and Broussard, C. (2007). What's new in psychtoolbox-3. *Perception* 36, 1–16.

Leemans, A., and Jones, D. K. (2009). The B-matrix must be rotated when correcting for subject motion in DTI data. *Magn. Reson. Med.* 61, 1336–1349. doi: 10.1002/mrm.21890

Leemans, A., Jeurissen, B., Sijbers, J., and Jones, D. (2009). "ExploreDTI: A graphical toolbox for processing, analyzing, and visualizing diffusion MR data," in *17th Annual Meeting of Intl. Soc. Mag. Reson. Med.* 3537.

Leotti, L. A., and Wager, T. D. (2010). Motivational influences on response inhibition measures. *J. Exp. Psychol. Hum. Percept. Perform.* 36, 430–447. doi: 10.1037/a0016802

Logan, G. D., Cowan, W. B., and Davis, K. A. (1984). On the ability to inhibit simple and choice reaction time responses: a model and a method. *J. Exp. Psychol. Hum. Percept. Perform.* 10, 276–291. doi: 10.1037/0096-1523.10.2.276

Messel, M. S., Raud, L., Hoff, P. K., Skaftnes, C. S., and Huster, R. J. (2019). Strategy switches in proactive inhibitory control and their association with task-general and stopping-specific networks. *Neuropsychologia* 135:107220. doi: 10.1016/j. neuropsychologia.2019.107220

Pelli, D. G. (1997). The VideoToolbox software for visual psychophysics: transforming numbers into movies. *Spat. Vis.* 10, 437–442. doi: 10.1163/ 156856897X00366

Swann, N. C., Cai, W., Conner, C. R., Pieters, T. A., Claffey, M. P., George, J. S., et al. (2012). Roles for the pre-supplementary motor area and the right inferior frontal gyrus in stopping action: electrophysiological responses and functional and structural connectivity. *NeuroImage* 59, 2860–2870. doi: 10. 1016/j.neuroimage.2011.09.049

Tax, C. M. W., Otte, W. M., Viergever, M. A., Dijkhuizen, R. M., and Leemans, A. (2015). REKINDLE: robust extraction of kurtosis INDices with linear estimation. *Magn. Reson. Med.* 73, 794–808. doi: 10.1002/mrm. 25165

Tzourio-Mazoyer, N., Landeau, B., Papathanassiou, D., Crivello, F., Etard, O., Delcroix, N., et al. (2002). Automated Anatomical Labeling of Activations in SPM Using a Macroscopic Anatomical Parcellation of the MNI MRI Single-Subject Brain. *NeuroImage* 15, 273–289. doi: 10.1006/nimg.2001. 0978

van Belle, J., Vink, M., Durston, S., and Zandbelt, B. B. (2014). Common and unique neural networks for proactive and reactive response inhibition revealed by independent component analysis of functional MRI data. *NeuroImage* 103, 65–74. doi: 10.1016/j.neuroimage.2014.09.014

van Gaal, S., Ridderinkhof, K. R., Scholte, H. S., and Lamme, V. A. F. (2010). Unconscious Activation of the Prefrontal No-Go Network. *J. Neurosci.* 30, 4143–4150. doi: 10.1523/JNEUROSCI.2992-09.2010

Verbruggen, F., and Logan, G. D. (2009). Models of response inhibition in the stop-signal and stop-change paradigms. *Neurosci. Biobehav. Rev.* 33, 647–661. doi: 10.1016/j.neubiorev.2008.08.014

Verbruggen, F., Aron, A. R., Band, G. P., Beste, C., Bissett, P. G., Brockett, A. T., et al. (2019). A consensus guide to capturing the ability to inhibit actions and impulsive behaviors in the stop-signal task. *eLife* 8:e46323. doi: 10.7554/eLife.46323

Xu, B., Sandrini, M., Wang, W.-T., Smith, J. F., Sarlls, J. E., Awosika, O., et al. (2016). PreSMA stimulation changes task-free functional connectivity in the fronto-basal-ganglia that correlates with response inhibition efficiency. *Hum. Brain Mapp.* 37, 3236–3249. doi: 10.1002/hbm.23236

Zandbelt, B. B., and Vink, M. (2010). On the Role of the Striatum in Response Inhibition. *PLoS One* 5:e13848. doi: 10.1371/journal.pone.0013848